4.1 DESIGN OF EXPERIMENTATION FOR FLUX FORMULATION

Extreme vertices design approach of design of the experiment suggested by MecLean and Anderson was used for flux formulations [Cornell, 2002; Anderson and MecLean, 1974]. According to this method, a mixture of q components having lower and higher limits for all of the components may be represented by equation (4.1) and (4.2).

$$0 \leq \alpha_i \leq x_i \leq \beta_i \leq 100 \tag{4.1}$$

$$\sum\nolimits^{k}_{i=1} x_i = 100 \tag{4.2}$$

Where i= 1, 2, 3...., k and α_i and β_i are the lower and upper limits of constants on the x_i, which is the percentage composition of the ith component in the mixture. By satisfying lower and higher limits from $q.2^{q-1}$, the vertices of polyhedron were selected. While the two dimensional faces of polyhedron was found by combining vertices of polyhedron into three or more groups of vertices where every vertex having similar value x_i for one of the elements. The overall centroid selected by an average of all the centroids. Centroids of two-dimensional faces chosen as design points. The second-order regression model gives the output response characterstics (Equation 4.3):

$$Y = \sum\nolimits^{k}_{i=1} b_i x_i + \sum i < j \sum\nolimits^{k} b_{ij} x_i x_j \tag{4.3}$$

Where b_i and b_{ij} are least-square model regression coefficients, the terms $b_i x_i$ and $b_{ij} x_i x_j$ in the regression model shows the specific and mixed influence of the mixture constituents. In a mixture design approach, the independent factors are proportions of different components of a blend. Simplex lattice design and simplex centroid design are the standard mixture designs for fitting standard models when the mixture components are subject to the constraint that they must sum to one. The confined design space is easy to define in simplex design approach if there is no lower or upper limit on the constituents of the mixture, due to which all the point lies on or inside the region of a regular (k-1)-dimensional simplex. So the confined design space of k dimensions is reduced to (k-1)-dimensional simplex. Figure 4.1(a-c) shows the example of three constituent mixture (k=3) system (e.g. cube) is compressed to a two dimensional simplex system (equilateral triangle) and for quaternary system (k=4) it is reduced to tetrahedron (Figure 4.4). Extreme vertices design or constrained mixture design is appropriate to use other than the standard mixture designs when mixture constituents subjected to additional constraints such as minimum or maximum value for each component. In mixture experiments, the amount of mixture does not matter because the measured responses depend only upon the relative proportions of the constituents in the mixture. The primary purpose of mixture experiments is to model the mixture constituents in the form of mathematical equations. So that prediction of measured values for the combination of mixture constituents can be made empirically.
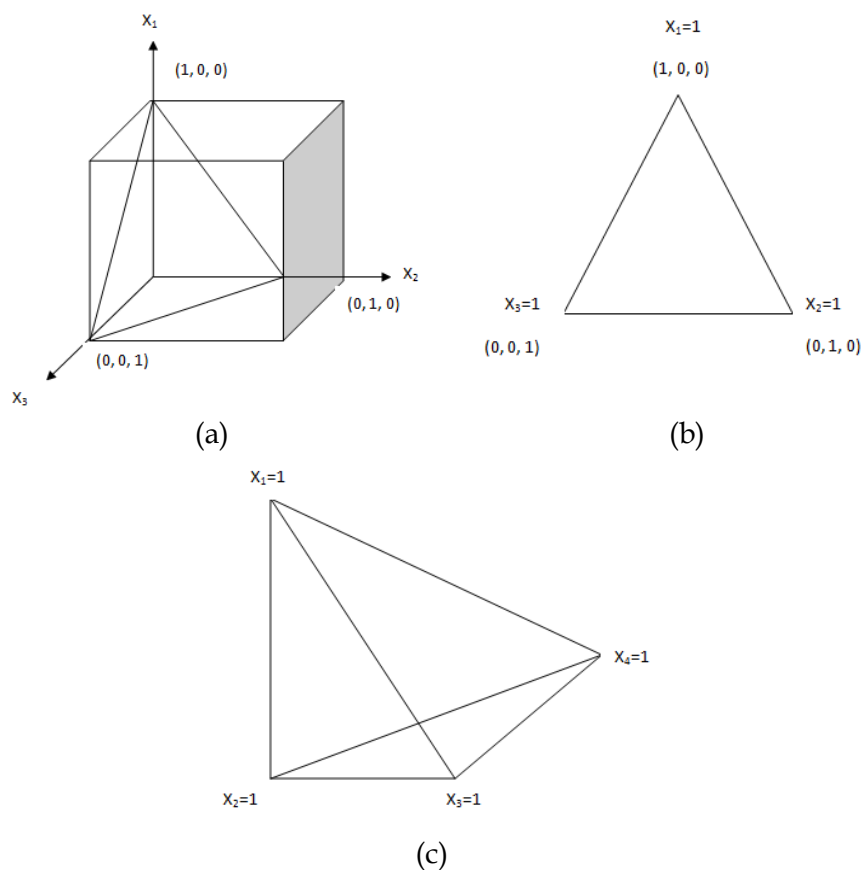
Figure 4.1: Confined design space as per simplex design; (a-b) three component regions; (c) tetrahedron component region [Cornell, 2002]

Using ANOVA or F-test for physicochemical or thermophysical properties the various regression models were analyzed. By calculating F and P values at 95% significance level the adequacy of different models was checked [Montgomery, 2008]. By using hypothesis testing through ANOVA or F-test the developed regression models were analyzed for linear, quadratic and ternary terms. Table 4.1 shows the calculation of ANOVA F_0-value using hypothesis analysis [Montgomery, 2008, Box et al., 2005, Montgomery and Runger, 2010].

Table 4.1: Significance of regression using ANOVA

Variation type	SS	DOF	MS	F_o
Regression	SS_R	k	$MS_R = SS_R/k$	MS_R / MS_E
Error	SS_E	n-k-1	$MS_E = SS_E/n-k-1$	
Total	SS_T	n-1		

Note: SS: Sum of square; MS: Mean sum of square; DOF; degree of freedom; n= no of experiments; k= no of regression variables

Tabulated F ($F_{\alpha, k, n-k-1}$) and α value compared with calculated F values at 95% significance level. The null hypothesis is rejected (H_0 is rejected), or the model is significant if the calculated F_0 value is higher than the theoretical value, $F_{\alpha, k, n-k-1}$. The model is significant, or the null hypothesis rejected if the P-value for the statistic F_0 is less than α. Physical characteristics and more than one response can be observed for end products in most of the industrial processes or products which are under investigation at the same time. During process design, to obtain the best levels of factors, some responses must be optimized simultaneously. An analyst must decide which response is most suitable, although there is some common relationship between

these responses. The multi-objective, multi-variable, and non-linear optimization problem formulated in terms of maximizing or minimizing of target values of various responses. The composite desirability method suggested by [Derringer and Such 1980] is generally used to optimize output responses. Optimal parameter combinations considered for the factor settings with maximum total desirability [Harington, 1965]. In multi-objective optimization, weights are used to fix the importance of an objective. With a certain degree of degradation in the performance of one objective, there is a greater improvement in the performance of the other objective if the weight of that objective is higher. Mathematical relation for composite desirability is given by equation (4.4) and (4.5).

$$D = [d_1^{w_1} . d_2^{w_2} .... d_n^{w_n}]^{1/(w_1 + w_2 + ... w_n)} \qquad (4.4)$$

$$D = [\prod\nolimits^{i \to n} d_i]^{1/\sum_{i \to n} w_i} \qquad (4.5)$$

Where d_i is the desirability of specific response, n is the number of responses and w_i are the weights satisfying $0 < w_i < 1$ and $(w_1 + w_2 + w_3 + ... + w_n) = 1$.

4.1.1 Selection of welding process parameters

Submerged arc welding comprises various process variables such as welding current, welding voltage, welding speed, nature of flux, nature of filler wire, filler electrode size, etc. Welding current, voltage, and speed are the main process parameters that frequently used in the submerged arc welding process. Filler wire diameter, nature of flux, flux grain size, type of current polarity, and the angle between work-piece and electrode affects the weld bead morphology [Jindal et al., 2013].

1) Welding current:

The deposition rate, rate of filler electrode melted, parent metal melted, and the penetration depth are mostly affected by the welding current parameter. Melting rate as well as penetration rate increases with the increase in current. Undercuts observed in the weld deposits at excessively high welding current, which results in digging arc.

2) Welding voltage:

Welding voltage primarily controls the arc length which is the distance between the molten weld pool and the wire filler metal at the point of melting within the arc. As the voltage is increased, the weld bead will flatten out more and have an increasing width-to-depth ratio. As the arc length increases proportional to an increase in voltage, the electrode extension, distance from the contact tip to the point where the welding wire is melting in the arc, consequently decreases. As the electrode extension decrease so also does the resistance to the welding current flowing through that portion of the wire decreased. More heat is available to melt the metal or flux with increase in voltage, which increases the arc length, respectively. At high voltage, generally wider and concave weld beads produced in the groove welds. Chances of formation of undercuts along the edges of fillet weld increases at high voltage. In deep weld grooves, penetration improved at lower welding voltage, which results in a stiffer arc and retards arc blow. Too low voltage results narrow bead formation, which causes difficulty in slag removed along the edges.

3) Welding speed:

If there is an increase in the travel speed, then there is a decrease in the heat input per unit length of the weld. It causes the melting rate of filler wire to decrease, which results in less weld reinforcement. The size of the weld bead formed is smaller due to less weld reinforcement.

Uneven bead shape, porosity, undercutting, and arc blow occurs at excessively high welding speed. Cracking and excessive exposure to the arc is uncomfortable for the welding operator if the rough or convex bead formed, which results due to the reason of lower welding speeds. To decide the welding process variables for experimentation, welding trials conducted. The following specifications used for submerged arc welding machine:

Specification	Range
Welding Current	350-450 Ampere
Arc Voltage	31±1 Volt
Speed	6.0 mm/s
Wire size	3.2 mm
Duty cycle	100% (at 450 ampere)
Efficiency	≥0.95

To assess the bead profile, and slag detachability various pre trials were carried out. On low, medium and high scale arc stability and slag detachability were qualitatively accessed. On low scale there is larger the magnitude of voltage fluctuation (e.g. ± 4 V), due to which the greater is the arc instability while a stable arc fluctuates between ±1 V and will produce good weld bead and a defect free weld nugget. The arc should initiate easily and be able to maintain itself under a varying arc length. For a basic flux system, flux no. 1 is selected for pre-trials of multi-pass bead on plate experimentation, and Table 4.4 & Figure 4.4 represents the vertex of the design matrix. Flux 1 is chosen to decide the suitable welding current, voltage, and speed during pre-trials. Multi-pass bead on plate experiments was performed using direct current electrode positive (DCEP) polarity and constant speed 6 mm/s. Table 4.2 shows the qualitative behavior observed and marked using current and voltage range. For further investigations of the basic flux system, the current value of 450 amperes, voltage 32 volts, and the welding speed of 6 mm/s shows better qualitative observations. The same procedure repeated for rutile-basic and rutile-acidic flux systems at 450A current, 32V voltage, and 6 mm/s speed, respectively. It observed that almost similar results obtained like that of a basic flux system. So using 450A current, 32V voltage, and 6 mm/s speed, further investigations of rutile-basic and rutile-acidic flux systems were carried out.

Table 4.2: Qualitative observations for basic flux system (using flux no.1)

S.NO	Current (A)	Voltage (V)	Speed (mm/s)	Slag detachability	Arc stability	Bead appearance
1.	350	30	6	Poor	Poor	Poor
2.	350	31	6	Poor	Poor	Poor
3.	350	32	6	Poor	Medium	Poor
4.	400	30	6	Medium	Medium	Moderate
5	400	31	6	Medium	Medium	Moderate
6	400	32	6	Medium	Medium	Moderate
7.	450	31	6	Good	Good	Good
8.	450	31	6	Good	Good	Good
9.	450	32	6	Good	Good	Good

Bead width and bead height are the two main characteristics of the weld bead, as shown in Figure 4.2. To ensure that the weld joint is adequately filled or free from defects, bead width, and bead height are essential parameters to show bead morphology. Excessive bead height results in the difficulty of making proper weld passes due to a lack of fusion. Poor fusion may occur due to the formation of narrow and excessive peaked weld bead.
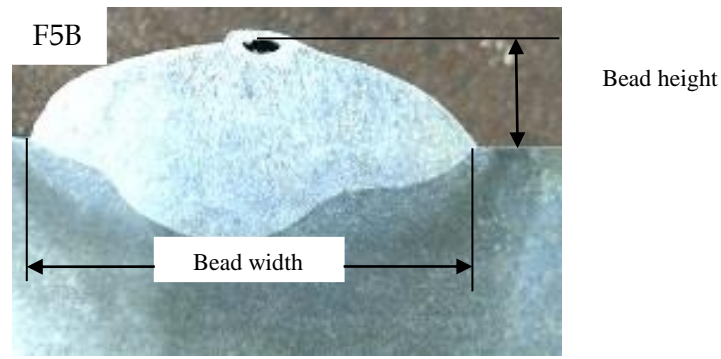
Figure 4.2: Bead profile observed for basic flux at 450 Amp, 32 V and 14 inch/min welding parameters (flux no. 5 F5B)

In present work, different mineral constituents silica, calcite, rutile, fluorspar, talc, calcinated bauxite, and potassium silicate used in different proportions as flux formulations for three flux systems (e.g., basic, rutile basic and rutile acidic flux systems). The elemental chemical composition of each mineral component is calculated using the X-ray fluorescence (XRF) technique available at Defence Laboratory, Jodhpur. Table 4.3 shows the individual weight percentage of mineral elements used for flux preparation. For flux formulation, in each flux system like a basic flux system, four different mineral constituents (e.g., calcite, silica, fluorspar and calcinated bauxite) and potassium silicate were used as a binder in a constant proportion. After flux preparation, physicochemical and thermophysical properties of submerged arc welding fluxes such as density, grain fineness number, thermal conductivity, thermal diffusivity, specific heat, percentage weight change, and change in enthalpy was evaluated. Density and grain fineness number of fluxes evaluated at room temperature. By using formulated fluxes (for three flux systems), the multi-pass bead on plate weld deposits performed at optimum welding parameters. Two fluxes from each flux system selected by qualitative analysis of beads and submerged arc welding were performed using these fluxes. Tensile strength, impact strength, microhardness, microstructure and hydrogen induced cracking characterization of weld specimens was performed.

Flux plays mainly important role during submerged arc welding, some of are:
- Calcite is basic in nature and CaO is its main source. CaO is a very stable oxide. It helps in improving impact strength of weld metal by removing sulphur and phosphorous impurities [Chai et al., 1982].
- Al_2O_3 is an eesential flux component, and its primary source is calcinated bauxite. It helps in the formation of acicular ferrite microstructure which is known to have good mechanical properties. A ferrite needle having interlocking nature with fine grains provides maximum crack propagation resistance [Lau et al., 1986].
- TiO_2 is a neutral component, and its primary source is rutile. It provides excellent slag detachability due to the transfer of titanium from TiO_2 to weld metal.
- The formation of hydrogen fluoride can reduce dissolved hydrogen present in the molten weld metal. Fluorspar is the main source of CaF_2 and used as a basic flux element.
- To reduce the formation of oxygen in the weld metal magnesium oxide (MgO) is very useful for increasing the basicity of the slag. Too high increase in MgO content (>40%) in the weld metal produces unstable arc and causes slag entrapment in the weld metal. Talc is the primary source for MgO.
- Silica is the main source for SiO_2 and is a suitable slag improving agent when used as welding flux. In a molten state, SiO_2 provides proper viscosity and good current-carrying capacity to the welding flux [J.H. Palm, 1979; Paniagua et al., 2003 and 2009].

The composite melting temperature of flux should be lower than that of base metal because flux should melt first and remain in molten form after solidification of the weld metal to provide

atmospheric contamination [Bhandari et al., 2012]. According to this aspect, the ternary phase diagrams for three flux systems i.e., basic, rutile basic, and rutile acidic flux systems, were analyzed. Based on ternary diagrams, the percentage composition of flux elements was selected [Zhao et al., 2004]. Figure.4.3(a, b, c) shows the ternary phase diagrams for basic (CaO-SiO_2-CaF_2), rutile basic (TiO_2-SiO_2-CaO) and rutile acidic (TiO_2-SiO_2-MgO) flux systems [J. Mukerji et al., 1965, Eriksson G et al., 1993, De Vries et al., 1955]. According to the available literature, the range of the flux ingredients is further narrowed in all three flux systems. In each flux system (i.e., basic, rutile basic, and rutile acidic flux system), four flux constituents mixed as per the following constraints (Equations 4.6 or 4.7 for the basic system, 4.8 or 4.9 for rutile basic and 4.10 or 4.11 for rutile acidic flux system). By varying the composition of four flux components and keeping binder content constant in each flux system (e.g., CaO, SiO_2, CaF_2, and Al_2O_3 in the basic system), twenty-one agglomerated fluxes were prepared using extreme vertices design approach shown in table 4.4. Figure.4.4 shows the polyhedron having six vertices, nine center edges, five plane centers, and one overall centroid formed in mixture designing of flux ingredients. In a mixture design approach out of 32 combinations (q.2q-1 = 4.24-1 = 32), six vertices of polyhedron selected in such a way that four elements were satisfying lower and higher limits (Figure 4.4). By grouping the vertices of a polyhedron into groups of three or more vertices, the two-dimensional faces of polyhedron were selected. Fourteen such combinations made in which polyhedron having nine center edges and five plane centers formed. The centroid of the triangular faces of polyhedron taken as design points. A total of twenty-one experiments performed for three flux systems. The design matrix for flux formulation for three flux systems is shown in table 4.4-4.6.

$$25 \le CaO\ (x_1) \le 40$$
$$10 \le SiO_2\ (x_2) \le 25$$
$$10 \le CaF_2\ (x_3) \le 25$$
$$5 \le Al_2O_3\ (x_4) \le 10 \tag{4.6}$$

$$\sum\nolimits_{i=1}^{4} x_i = 85 \tag{4.7}$$

$$25 \le TiO_2\ (x_1) \le 35$$
$$10 \le SiO_2\ (x_2) \le 25$$
$$15 \le CaO\ (x_3) \le 30$$
$$5 \le Al_2O_3\ (x4) \le 10 \tag{4.8}$$

$$\sum\nolimits_{i=1}^{4} x_i = 85 \tag{4.9}$$

$$30 \le TiO_2\ (x_1) \le 40$$
$$10 \le SiO_2\ (x_2) \le 20$$
$$15 \le MgO\ (x_3) \le 25$$
$$5 \le Al_2O_3\ (x_4) \le 10 \tag{4.10}$$

$$\sum\nolimits_{i=1}^{4} x_i = 85 \tag{4.11}$$

(a)

(b)

(c)

Figure 4.3: Experimental Ternary phase diagrams for, (a) basic system; (b) rutile basic system; (c) rutile acidic system (J. Mukerji et. al., 1965, Eriksson G et al., 1993, De Vries et al., 1955).

Figure 4.4: 3D-polydehedron designed as per mixture design approach for flux formulation

Table 4.3: Elemental chemical analysis of mineral components

Element (Wt. %)	Al	Si	Ca	Ti	Fe	Mg	S	P
Silica	2.82	96.16	0.48	--	0.17	--	0.29	--
Rutile	5.94	4.09	1.45	87.46	1.52	--	--	0.492
Calcinated bauxite	82.2	6.90	2.50	3.80	3.50	--	--	--

	CaO	SiO₂	CaF₂					
Talc	11.70	35.00	--	--	--	54.05	0.03	0.09
Calcite	4.61	2.95	81.45	--	0.74	9.48	--	--
Fluorspar	4.97	1.38	92.77	--	0.41	--	--	--

Table 4.4: Design matrix for basic flux formulation

Exp. No	Basic Flux	Basicity Index	Nature of polyhedron points	Ingredients of flux constituents (wt. %)			
				CaO	SiO₂	CaF₂	Al₂O₃
1	F1	2.4	Vertex	40.0	10.0	25.0	10.0
2	F2	2.1	Vertex	40.0	15.0	25.0	5.0
3	F3	3.6	Vertex	40.0	18.75	18.75	7.5
4	F4	2.9	Vertex	30.0	25.0	25.0	5.0
5	F5	2.2	Vertex	36.66	21.66	21.66	5.0
6	F6	2.1	Vertex	35.83	20.83	20.83	7.5
7	F7	1.8	Centre Edge	40.0	25.0	10.0	10.0
8	F8	2.4	Centre Edge	33.75	18.75	25.0	7.5
9	F9	2.0	Centre Edge	35.0	20.0	20.0	10.0
10	F10	1.8	Centre Edge	33.75	25.0	18.75	7.5
11	F11	1.7	Centre Edge	25.0	25.0	25.0	10.0
12	F12	1.9	Centre Edge	40.0	25.0	15.0	5.0
13	F13	1.6	Centre Edge	32.5	25.0	17.5	10
14	F14	1.2	Centre Edge	32.5	17.5	25.0	10
15	F15	2.0	Centre Edge	40.0	12.5	25.0	7.5
16	F16	2.6	Plane Centre	40.0	17.5	17.5	10
17	F17	1.78	Plane Centre	40.0	25.0	12.5	7.5
18	F18	1.92	Plane Centre	35.0	25.0	20.0	5.0
19	F19	2.5	Plane Centre	40.0	20.0	20.0	5.0
20	F20	1.78	Plane Centre	27.5	25.0	25.0	7.5
21	F21	2.46	Overall Centroid	35.0	20.0	25.0	5.0

Table 4.5: Design matrix for rutile-basic flux formulation

Exp. No	Rutile- basic flux	Basicity Index	Nature of polyhedron points	Ingredients of flux constituents (wt. %)			
				TiO₂	SiO₂	CaO	Al₂O₃
1	F1	1.5	Vertex	20.0	25.0	30.0	10.0
2	F2	1.0	Vertex	35.0	17.5	22.5	10.0
3	F3	1.2	Vertex	30.0	20.0	25.0	10.0
4	F4	1.3	Vertex	35.0	25.0	17.5	7.5
5	F5	1.0	Vertex	35.0	10.0	30.0	10.0
6	F6	0.96	Vertex	35.0	25.0	20.0	5.0
7	F7	0.7	Centre Edge	31.66	21.66	26.66	5.0
8	F8	1.0	Centre Edge	25.0	25.0	30.0	5.0
9	F9	1.1	Centre Edge	27.5	17.5	30.0	10.0
10	F10	0.89	Centre Edge	35.0	18.75	23.75	7.5
11	F11	0.94	Centre Edge	30.0	25.0	25.0	5.0
12	F12	1.2	Centre Edge	30.83	20.83	25.83	7.5
13	F13	0.85	Centre Edge	35.0	15.0	30.0	5.0
14	F14	0.7	Centre Edge	28.75	25.0	23.75	7.5
15	F15	1.0	Centre Edge	35.0	25.0	15.0	10.0
16	F16	0.90	Plane Centre	30.0	20.0	30.0	5.0

17	F17	1.3	Plane Centre	22.5	25.0	30.0	7.5
18	F18	0.93	Plane Centre	35.0	20.0	25.0	5.0
19	F19	1.0	Plane Centre	35.0	12.5	30.0	7.5
20	F20	1.1	Plane Centre	27.5	25.0	22.5	10
21	F21	0.7	Overall Centroid	28.5	18.75	30.0	7.5

Table 4.6: Design matrix for rutile-acidic flux formulation

Exp. No	Rutile-acidic flux	Basicity Index	Nature of polyhedron points	Ingredients of flux constituents (wt. %)			
				TiO_2	SiO_2	MgO	Al_2O_3
1	F1	0.63	Vertex	36.66	16.66	21.66	10.0
2	F2	0.77	Vertex	37.50	17.50	22.50	7.5
3	F3	0.69	Vertex	40.0	12.5	25.0	7.5
4	F4	0.74	Vertex	40.0	20.0	17.5	7.5
5	F5	0.78	Vertex	40.0	10.0	25.0	10.0
6	F6	0.74	Vertex	36.25	20.0	21.5	7.5
7	F7	0.71	Centre Edge	35.0	20.0	20.0	10.0
8	F8	0.60	Centre Edge	32.5	20.0	25.0	7.5
9	F9	0.66	Centre Edge	38.33	18.33	23.33	5.0
10	F10	0.48	Centre Edge	40.0	20.0	22.5	5.0
11	F11	0.60	Centre Edge	37.5	20.0	22.5	5.0
12	F12	0.83	Centre Edge	35.0	20.0	25.0	5.0
13	F13	0.70	Centre Edge	40.0	16.25	21.25	7.5
14	F14	0.58	Centre Edge	40.0	20.0	15.0	10
15	F15	0.76	Centre Edge	40.0	15.0	25.0	5
16	F16	0.65	Plane Centre	40.0	15	20.0	10
17	F17	0.72	Plane Centre	37.5	17.5	25	5
18	F18	0.73	Plane Centre	30.0	20.0	25	10
19	F19	0.64	Plane Centre	40.0	17.5	22.5	5.0
20	F20	0.52	Plane Centre	36.25	16.25	25	7.5
21	F21	0.77	Overall Centriod	35.0	15.0	25	10

4.2 SUBMERGED ARC WELDING FLUX PREPARATION

Submerged arc welding flux preparation involves the following steps:

By using digital weighing balance (accuracy 1mg), different mineral components of welding flux were weighed separately as per the weight percentage is taken in Table 4.4-4.6. To get homogeneous solid mass, these weighed mineral components were mixed thoroughly for thirty minutes with potassium silicate (app. 20%) binder [Houldcroft, 1989; Houldcroft, 1977; Singh & Pandey, 2008; Singh & Pandey 2009; Kumar et al., 2009; Kumar et al., 2010]. For better arc stability and proper binding of individual flux components, a potassium silicate binder used. After drying in the air for a few hours, the solid mass is baked in a muffle furnace at 200º C for one hour. To completely remove the moisture, the solid mass was sintered at 900º C in the furnace for three hours. After sintering, the flux mass was allowed to cool, then crushed, sieved, and packed in air-tight packets [Golovko et al., 2011].

4.3 PHYSICOCHEMICAL AND THERMOPHYSICAL CHARACTERIZATION OF SAW FLUXES (FOR THREE FLUX SYSTEMS)

After flux preparation, physicochemical and thermophysical properties of submerged arc welding fluxes such as density, grain fineness number, thermal conductivity, thermal diffusivity, specific heat, percentage weight change and change in enthalpy evaluated. Density and grain fineness number of fluxes was evaluated at room temperature. While thermal properties were evaluated by using simultaneous thermal analyzer and hot-disc techniques.

4.3.1 Density measurement of fluxes

Density of formulated fluxes (for three flux systems) was evaluated at room temperature using tabbed density method. In this method, for density measurement 10ml cylindrical flask was taken and for weight measurement weighing balance of capacity 200 gm was taken (1 ml = 1 cm^3). Density was calculated by equation (4.12) given below.

$$\text{Density} = \frac{\text{Mass}}{\text{Volume}} \tag{4.12}$$

4.3.2 Grain finesses number (GFN) calculation

Grain finesses number (GFN) is the measure of the average grain size of particles in a powder sample and developed by American foundrymen's society (AFS). Grain finesses number of different fluxes (for three flux systems) found by using the sieve shaker apparatus. In this apparatus, different sieves of varying mesh sizes (vary up to micron level) used. A total of eleven sieves with decreasing mesh size used for the grain fineness number calculation. Top sieve is coarse while the bottom sieve is fine. The grain size determined by stirring a known amount of grains of different sizes in a downward direction through a set of standard sieves. The amount remaining in each sieve weighed after stirring for 10-15 minutes. The percentage amount of grains that retained in each sieve then calculated. Each sieve has given a multiplying factor, and the calculated percentage amount of grains multiplied with that multiplying factor, and then the product divided with the total percentage, which gives AFS grain finenesses number. As per AFS, formula to calculate grain fineness number given by equation (4.13).

$$\text{GFN} = \frac{\text{Summation of AFS product} \ (\sum F\ )}{\text{Summation of mass present in each sieve} \ (\sum C)} \times 0.5 \tag{4.13}$$

where $\sum$F is the sum of AFS product and $\sum$C is the sum of the mass (gm) present in each sieve mesh.

4.3.3 Weight loss and Change in enthalpy measurement

The thermogravimetric technique (TGA) was used to find the thermal stability of submerged arc welding fluxes (for three flux systems) in terms of percentage weight change. The thermogravimetric analyzer observes the weight change of specimens (mass loss or gain) as a function of temperature and time in a nitrogen gas atmosphere. During thermogravimetric analysis (Perkin Elmer 6000 STA), the temperature of the specimen is raised gradually in a furnace, and specimen weight change (loss or gain) is measured. To find the thermal stability, twenty-one submerged arc welding fluxes (for three flux systems) are simultaneously heated in a controlled furnace environment having a temperature range 25° C to 900° C at a constant heating rate (20° C/min). Perkin Elmer 6000 STA apparatus was also used to estimate the change in enthalpy of submerged arc welding fluxes. To calculate the change in enthalpy (for

three flux systems), submerged arc welding fluxes were heated in a controlled furnace at a temperature range of 25°C to 900° C with a constant heating rate of 20° C/min.

4.3.4 Thermal properties (e.g. thermal conductivity, thermal diffusivity and specific heat) measurement

For basic, rutile-basic, and rutile-acidic flux systems, hot-disc technique was used to estimate the thermal properties of submerged arc welding fluxes. The hot-disc method works on the principle of heat conduction in which specimen (e.g., powder sample) tightly placed in between two dies. A Kapton sensor (size 3.415 mm) placed in between the two dies for temperature measurements. Thermal properties such as thermal conductivity, thermal diffusivity, and specific heat measured at room temperature.

4.3.5 Contact angle and surface tension measurements

The wetting and surface tension properties of submerged arc welding fluxes (for three flux systems) studied by measuring the contact angle between the solid/liquid interfaces. The contact angle of twenty-one fluxes measured at 1378K, 1638K &1723K in the muffle furnace using the sessile drop method. The temperature range selected according to the composite melting temperature of the fluxes (for three systems, shown in fig.4.3). Due to that reason wettability of fluxes was studied at 1378K, 1638K &1723K temperature. To avoid the oxidation of heating substrate with the welding flux, a constant heating rate was used to attain the target temperature. By using image-J software, the contact angle, as well as the spreading area of the fluxes, was measured. To ensure the reproducibility and to maintain standard deviation within limits, at least three times the contact angle measurements were performed in the present study. As per the calculated contact angle value, different surface tension values for three flux systems were determined using Young's & Boni's equations. Various surface tension properties at different phases, such as liquid-solid, solid-gas, or liquid-gas interfaces of the heating substrate, can be evaluated using Young's equation 4.14 [Young et al., (2007)]. Using Dupre's equation (4.16), the adhesion energy of fluxes (for three flux systems) calculated.

$$y_{SL} = y_{SG} + y_{LG} \cos \theta \qquad (4.14)$$

where θ-contact angle; y_{LS} & y_{SG} - interfacial tensions (mN/m) at the solid-liquid and solid-gas interfaces respectively while y_{LG} - molten slag surface tension. According to Boni's mathematical expression, the surface tension of molten flux (y_{LG}) can be determined by equation 4.15 [Yanhui et al, (2014)]. Previous literature was used to find the surface tension factor, which given in table 4.7.

$$y_{LG} = x_1 f_1 + x_2 f_2 + x_3 f_3 + \ldots\ldots\ldots\ldots\ldots x_t f_t \qquad (4.15)$$

$$W_a = \gamma_{LG} * (1 + \cos \theta) \qquad (4.16)$$

$y_{LG=}$ surface tension, mN/m
x_t= percentage mole fraction of component t (%)
f_t = for t component surface tension factor, mN/m
W_a = work of adhesion (J/m^2)

**Table 4.7:** Previous references shows the surface tension factor (f_t) for different oxides

Oxides	Dependence of surface tension on temperature (K) or	References

	Surface tension factor (f_t)	
CaO	791-0.0935*T	[Yanhui et al, (2014)]
Al$_2$O$_3$	1024-0.177*T	[Yanhui et al, (2014)]
SiO$_2$	243.2+0.031*T	[Yanhui et al, (2014)]
CaF$_2$	407.75-0.07*T	[Shigeta et al, (1989)]
TiO$_2$	1384.3-0.6254*T	[Yanhui et al, (2014)]
MgO	1770-0.636*T	[Yanhui et al, (2014)]

Figure 4.5 (a-b) shows the initial and final stage of the flux pallet in the muffle furnace. Figure 4.6 shows the contact angle measuremt of various flux pallets after cooling in the open environment.
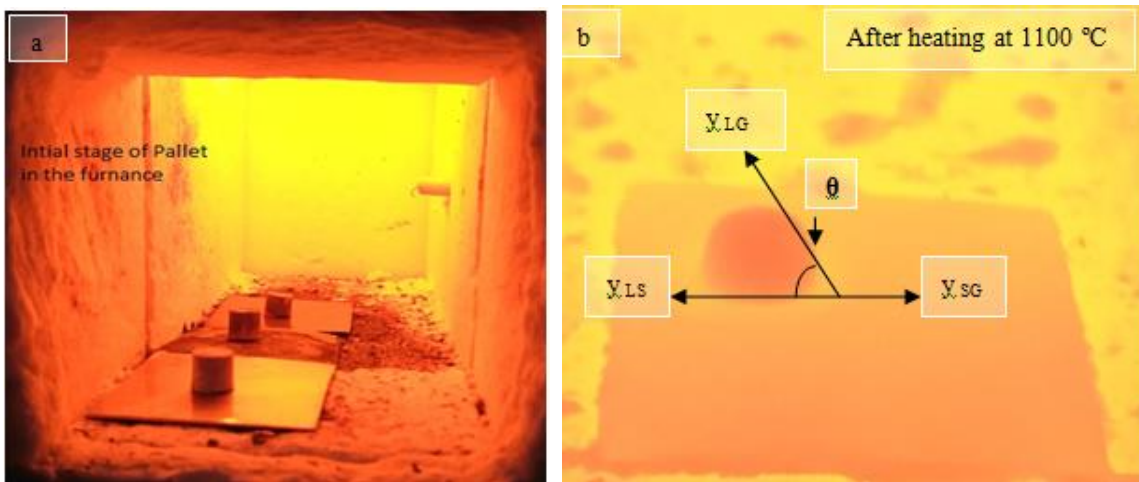
Figure 4.5: (a) Schematic representation of the horizontal muffle furnace; (b) macro-appearance of molten flux drop above the heating plate.
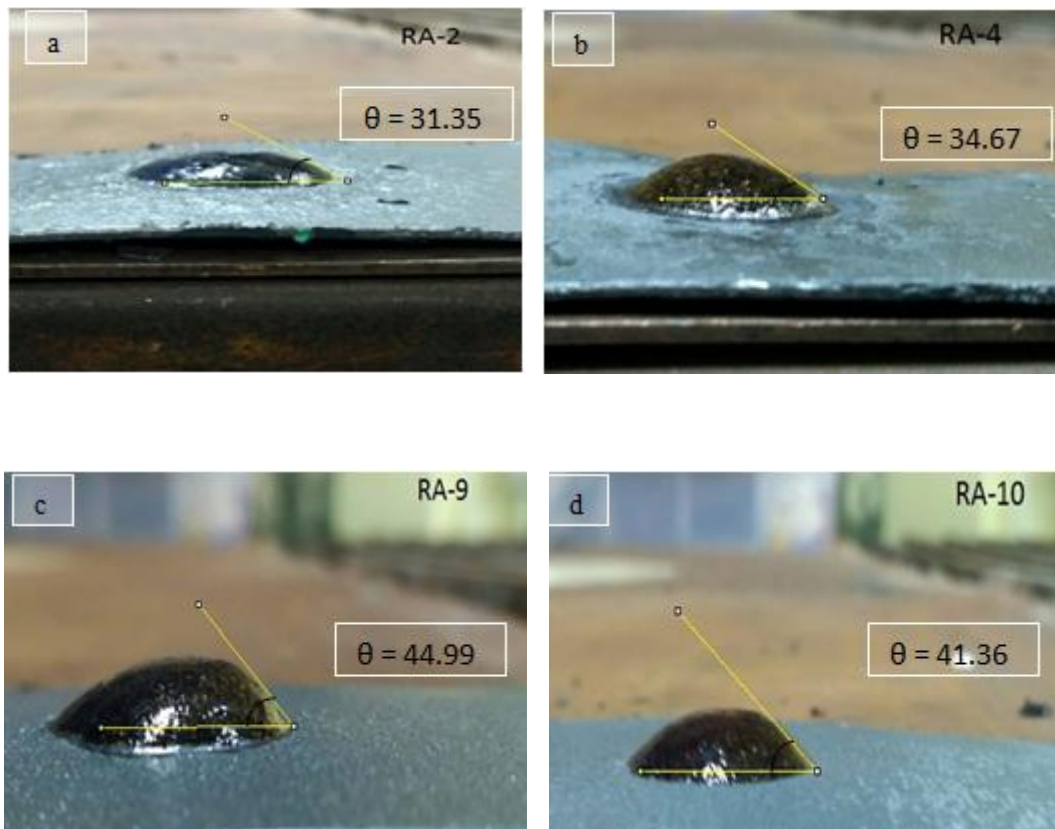
Figure 4.6: Contact angle measurement of various flux pallets (For rutile-acidic system)

4.3.6 Phase analysis of submerged arc fluxes

Bruker D-8 advance powder X-ray diffractometer was used to study the phase behaviour of basic, rutile-basic and rutile-acidic flux systems.

4.3.7 Structural analysis of submerged arc fluxes

Bruker Vertex 70v FTIR spectrometer was used to study the structural behavior of basic, rutile-basic, and rutile-acidic flux systems. FTIR analysis for three flux systems performed at a resolution of ± 2cm-1 in the wavenumber range of 400-4000 cm-1. FTIR spectrometer provides information regarding different bonds such as single, double, and triple bonds present in basic, rutile-basic, and rutile-acidic flux systems.

4.4 MULTI-PASS BEAD ON PLATE WELD DEPOSISTS EXPERIMENTATION USING SAW FLUXES

4.4.1 Multi-pass bead on plate experimentation for three flux system

Multi-pass bead on plate weld deposits experimentation performed (Figure 4.7) (for three flux systems) on submerged arc welding machine available at Jindal SAW Limited, Mundra. API X70 grade steel having dimensions 290 x 290 x 22 mm was used for a multi-pass bead on plate weld deposits experimentation. Pre-trials were carried out to select suitable welding parameters (Section 4.1.1). Based on pre-trial runs, the following welding parameters were chosen to perform multi-pass testing for three flux systems.

Welding Parameters	Unit
Current	450 A
Voltage	32 V
Speed	6 mm/sec
Wire diameter	3.2 mm (EA2TiB)
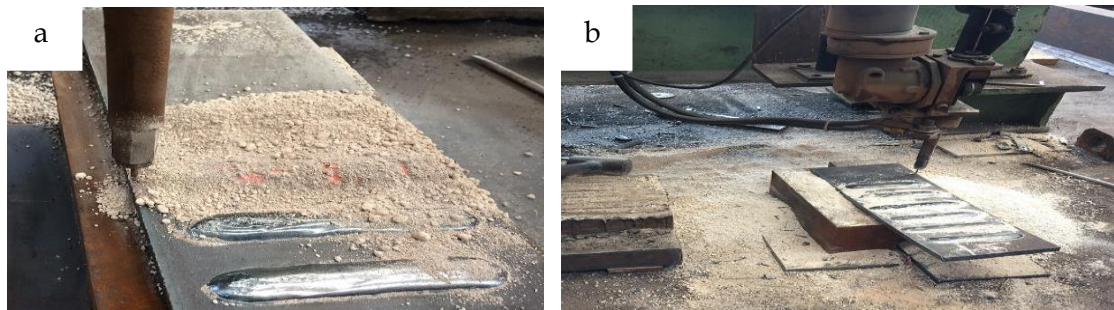
Figure 4.7: Steps of multi-pass bead on plate weld deposits experimentation using SAW machine.

4.4.2 Chemical analysis of beads for three flux systems

Optical emission spectrometer was used to evaluate the chemical behaviour of multi-pass bead on plate weld deposits for basic, rutile-basic and rutile-acidic flux systems.

4.4.3 Average Grain size and microhardness measurements of beads

An optical microscope was used to find the average grain size (ASTM E1368/ASTM E112) of multi-pass bead on plate weld deposit specimen. Microhardness tester was used to evaluate the microhardness (ASTM E384) of basic, rutile-basic and rutile-acidic flux systems at 1kg indentation load.

4.4.4 Selection of adequate flux by qualitatively analysing multi-pass weld deposits for three flux systems

Qualitatively analyzing beads (Figure 4.7) in terms of bead profile, porosity, and slag detachability, two adequate fluxes from each system i.e., basic, rutile-basic, and rutile-acidic flux system selected for final submerged arc welding. F5B, F15B, F5RB, F7RB, F3RA, and F19RA qualitatively selected for basic, rutile-basic, and rutile-acidic flux systems.

Note: F5B & F15B: basic flux system; F5RB & F7RB: rutile-basic flux system; F3RA & F19RA: rutile-acidic flux system.

4.5 MATERIAL & EXPERIMENTATION SETUP

The granular coating material, which is flux, covers the welding arc during the submerged arc welding process i.e., arc is submerged under the flux blanket. The excessive heat of welding arc between the filler electrode and workpiece produces coalescence of metals during the SAW process (Thomas, 1977; Lau et al., 1986). From the hopper, the dry granular flux is continuously fed through a tube in the arc region. To pick up the unfused flux to be used again, a vacuum system equipped in the automatic submerged arc welding machine.

Thick pipeline steel plates used in oil and gas industry nowadays welded by using automatic submerged arc welding machine as compared to manual and semiautomatic setup. Submerged arc welding consists of following process variables (Jindal et al, 2013):
1) Power source
2) Wire feeder or a control system
3) Automatic flux feeding head and mechanism
4) Travelling mechanism
5) Optional accessories

6) Fluxes and filler wires as main consumable material

1) Power source:

Either direct current (DC) or alternating current (AC) supply can be used in submerged arc welding process. In transformer-rectifier or a motor or a generator type setup direct current power source is used while alternating current is mainly used for transformer type and both types provide constant current and constant voltage outputs.

2) Wire feeder or a control system:

A simple wire feed speed control mechanism used in the semiautomatic submerged arc welding machine. Wire feeding speed is controlled with constant voltage power supplies, while arc voltage is monitored by constant current power supplies, which maintain a steady voltage while adjusting the wire feed speed.

3) Automatic flux feeding head and mechanism:

Feed roller assembly, torch setup, wire feeding assembly and various mounting accessories comprises the submerged arc welding head. To deposit the flux slightly ahead or concentric with the filler wire, a nozzle is generally mounted on the head. Flux hopper is generally mounted on the torch and flux feed on the base plate is due to gravity.

4) Travelling mechanism:

Important carriage mechanisms such as trolley type, tractor based or a side beam carriage type travelling mechanisms are used in submerged arc welding machine. Tractor based carriage mechanism is mostly used in submerged arc welding machine because straight movement as well as curvy movement can be performed due to easy handing or controlling.

5) Optional accessories:

A fixture, positioners and recovery units includes the optional accessories. Maximize flux utilization and minimizing manual usage by recalculating unused flux back in the hopper. Tilting rotating positioner, turning rolls and head-tailstock units are the commonly used positioners.

6) Fluxes and filler wires as main consumable material:

For various applications different types of electrode filler wires are manufactured to produce weld deposits matching the mechanical properties with the parent material such as carbon steel, alloy steel, stainless steel and special alloys. Copper coating of filler wires usually provides good shelf life, decreases wear and improves electrical conductivity. In submerged arc welding different sizes of electrode filler wires are used e.g. 1.6 mm to 6.4 mm in diameter. Flux play an important role in submerged arc welding process and it serves the following purposes (Chai et al., 1982):
  ➢ After melting flux floats on the molten metal and protects it from the atmospheric contamination by reducing oxygen and nitrogen pickup.
  ➢ Within the small welding zone flux concentrate heat and behave as a good insulator due to which proper fusion takes place between the filler wire and parent material.
  ➢ Flux add alloying elements such as titanium, copper, nickel and silicon in the weld metal
  ➢ Flux removes impurities such as sulphur and phosphorus from the weld metal and act as a cleaning agent.

- ➢ By decreasing spatter and burning losses the process efficiency is improved by submerged arc welding fluxes.

Two adequate fluxes from basic (F5B & F15B), rutile-basic (F5RB & F7RB) and rutile-acidic (F3RA & F19RA) flux systems were selected for submerged arc welding. Using adequate fluxes final weld experimentation was performed on submerged arc welding machine available at Jindal SAW Limited, Mundra.

Base and filler material: HSLA pipeline steel type and grade: API X 70 grade having 290 x 290 x 22 mm dimension, elemental composition of base and filler material was determined by optical emission spectrometer is given in table 4.8.

Table 4.8: Chemical composition of base metal and filler wire

Material	C	Si	Mn	P	S	Mo	Ni	Cr	Fe
BM (X70)	0.063	0.321	1.640	0.007	0.001	0.001	0.318	0.006	97.5
FW (EA2TiB)	0.029	0.088	0.871	0.010	0.007	0.216	0.084	0.032	98.4

Backing material: Material used for backing is API X70 having dimensions 300 x 300 x 6 mm.

4.6 SUBMERGED ARC WELDING AND VARIOUS CHARACTERIZATIONS USING ADEQUATE FLUXES FOR THREE FLUX SYSTEMS

4.6.1 Weld coupon preparation

Two API X70 grade steel specimens of size 145 x 145 x 22 mm was used for weld groove preparation. Figure 4.8 shows the weld coupon dimensions such as groove angle (θ), plate thickness (T_p), strip thickness (T_s) and width of plate (W).

Note: (W: width of plate=145mm; T_s: strip plate thickness =6mm; T_P: Plate thickness=22mm; $\theta°$= grove angle, 60°).
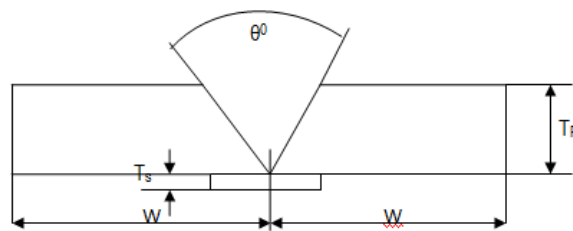
Figure 4.8: Weld coupon dimensions

4.6.2 Submerged arc welding of plates

Using adequate fluxes (taking two fluxes from three flux systems and one commercial flux) seven submerged arc weld coupons were fabricated utilizing two API X70 grade steel specimens of size 145 x 145 x 22 mm. Two API X70 steel plates were butt welded (Figure 4.9, a-c) on submerged arc welding machine available at Jindal SAW, Mundra (Gujarat). All experiments were performed using 3.2 mm diameter filler wire (EA2TiB) at optimum welding parameters (given in section 4.7.1). Welding of specimen was conducted by maintaining constant voltage mode with direct current reverse polarity and using constant wire feed rate.
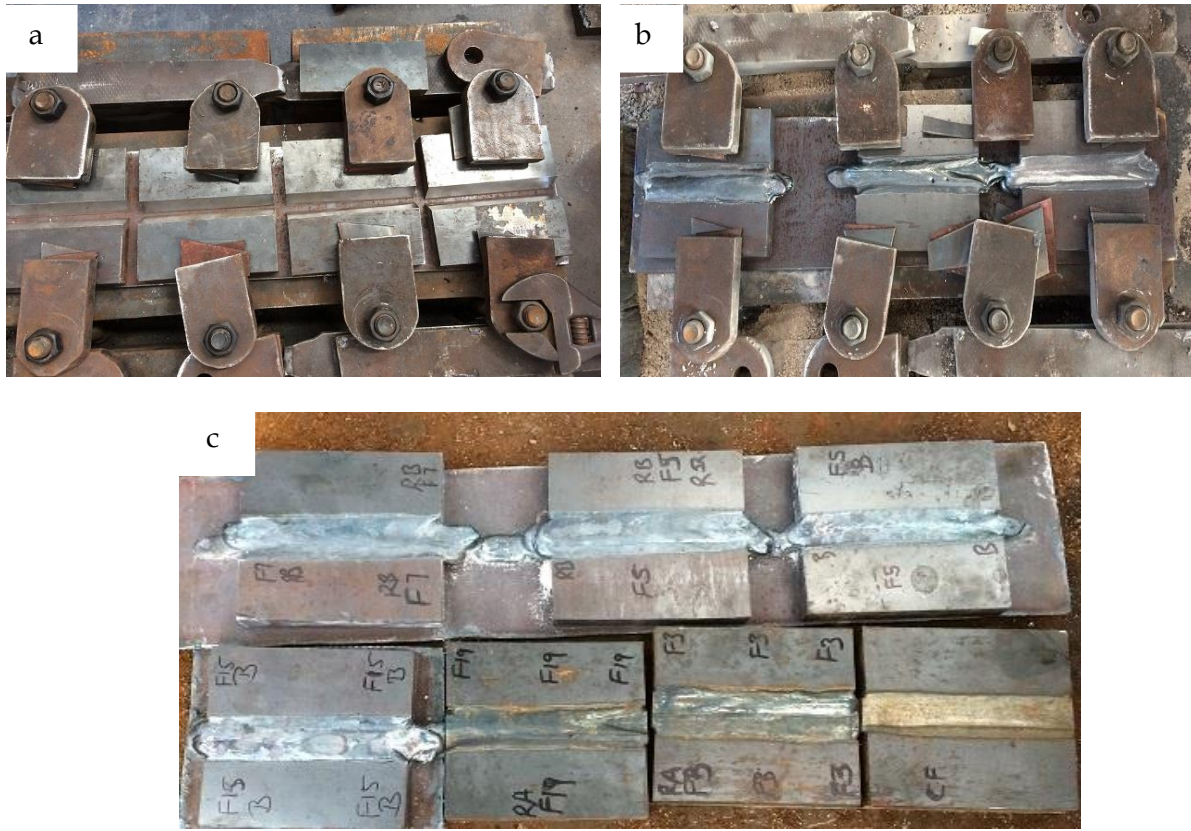
Figure 4.9: (a) Clamping of base plate specimens; (b) Conduction of submerged arc welding using adequate fluxes; (c) Seven submerged arc weldments.

4.6.3 Cutting of weld specimen

For different mechanical characterizations such as tensile testing, impact testing and microhardness testing, the weld specimens were cut along the transverse direction as shown in Fig.4.10.
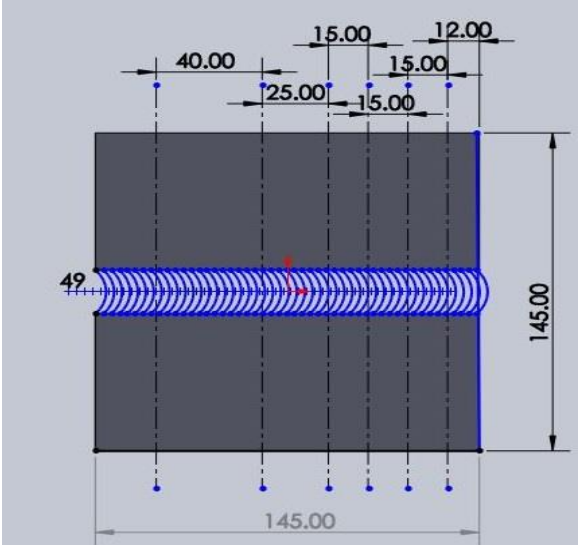

Figure 4.10: For different testing the arrangement of cutting specimens (All dimensions are in mm)

4.6.4 Mechanical characterization of weld specimen

For mechanical characterization and analysis of weld samples the specimen for tensile, impact and microhardness were cut as given in Fig.4.10.
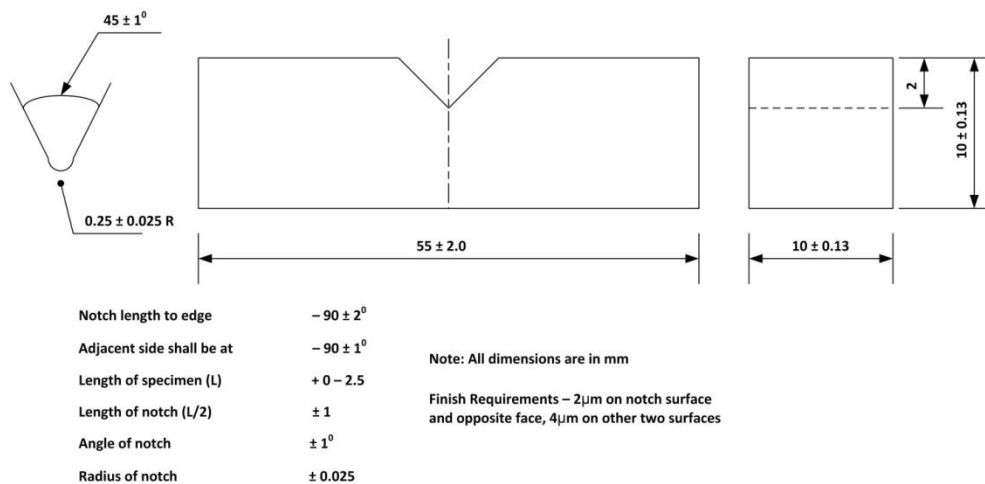
4.6.4.1 Tensile testing of weld specimens

Computerized UTM machine (UH-2000 KN X) available at Jindal SAW, Mundra was used to perform tensile testing of weld specimens (As per ASTM A387 standard). Figure 4.11 (a-b) shows the standard tensile specimen and actual tensile test specimens.
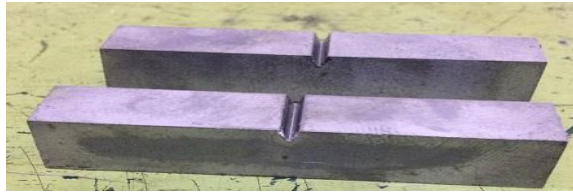

(a)   (b)
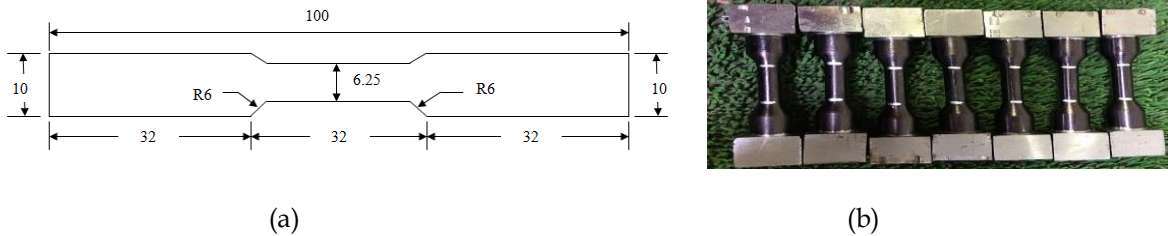
Figure 4.11: (a) Standard tensile test specimen (ASTM A387, all dimensions in mm); (b) Actual seven tensile test specimen.

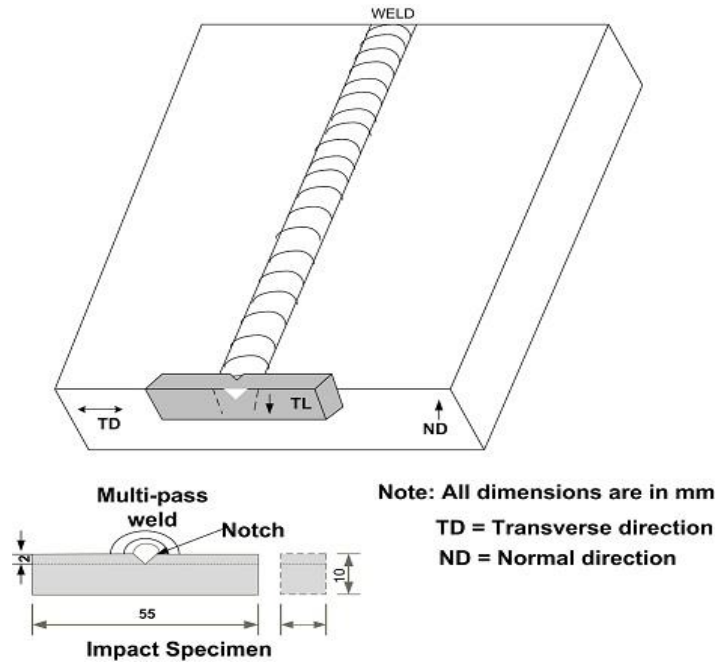#### 4.6.4.2 Impact testing of weld specimen

Impact testing of weld and HAZ specimens was performed on the impact testing machine available at Jindal SAW, Mundra, as per ASTM E23, 2001 standard. Figure 4.12 (a-b) shows the standard and actual impact test specimens. Impact testing of the weld, as well as HAZ specimens, performed at -65°C and room temperature. Standard 55 mm x 10 mm x 10 mm Charpy V-notch specimens, for the butt welds were situated in the transverse direction while a V-notch was prepared in the transverse-longitudinal (T-L) direction. This has been done to cover multi-passes of weld and comparatively greater region of weld zone as compared to the specimen with its notch aligned with the welding direction and into it. Due to this reason, across specimen with notch perpendicular to the welding direction gives better indication of impact energy [Notched bar Testing Part II – TWI; S.H. Hashemi]. The orientation and direction of the Charpy V-notch specimen in the weld zone is shown in Fig. 4.12(c).

Notch length to edge	– 90 ± 2°
Adjacent side shall be at	– 90 ± 1°
Length of specimen (L)	+ 0 – 2.5
Length of notch (L/2)	± 1
Angle of notch	± 1°
Radius of notch	± 0.025

Note: All dimensions are in mm

Finish Requirements – 2µm on notch surface and opposite face, 4µm on other two surfaces

(a)

(b)

(c)

Figure 4.12: (a) Standard impact test specimen; (b) Actual impact test specimen; (c) Orientation and direction of Charpy V notch in the weld zone.

4.6.4.3 Microhardness testing of welds specimen

Microhardness tester was used to evaluate the microhardness (ASTM E384) of weld specimens at a load of 1kg. Figure 4.13 shows the specimens for microharness testing of weld as well as HAZ samples.

Figure 4.13: Specimens for microhardness testing of weld and HAZ

4.6.5 Microstructural analysis of weld specimen

Dewinter optical microscope was used to find the microstructure of seven weld as well as HAZ specimens at 100X magnification.

4.6.6 Hydrogen induced cracking measurement of weld specimen

Structural integrity issues such as hydrogen-induced cracking generally observed for pipeline steels exposed in harsh environmental conditions. NACE TM0284-2003 standard is used to find the hydrogen-induced cracking behavior of weld specimens. According to NACE TM0284-2003 procedure, crack length ratio, crack sensitivity ratio, and crack thickness ratio quantitatively evaluated. By metallographic examination (at 100X magnification), these parameters were calculated. Figure 4.14 (a-b) shows the hydrogen-induced cracking set up available at Jindal SAW Limited, Mundra, and procedure to find the crack dimensions.

$$\text{Crack lenght ratio (CLR)} = \frac{\sum a \times 100\%}{W} \tag{4.17}$$

$$\text{Crack sensitivity ratio (CSR)} = \frac{\sum a \times b \times 100\%}{W \times T} \tag{4.18}$$

$$\text{Crack thickness ratio (CTR)} = \frac{\sum b \times 100\%}{T} \tag{4.19}$$

Where a is the crack length in the rectangular field, b is the crack width in the rectangular field, W is the width of the specimen and T is the thickness of the specimen. Here W=33mm, T=22mm, $\sum a$ and $\sum b$ can be calculated from section1 (S1) and section2 (S2) from Fig. 4.21(b).
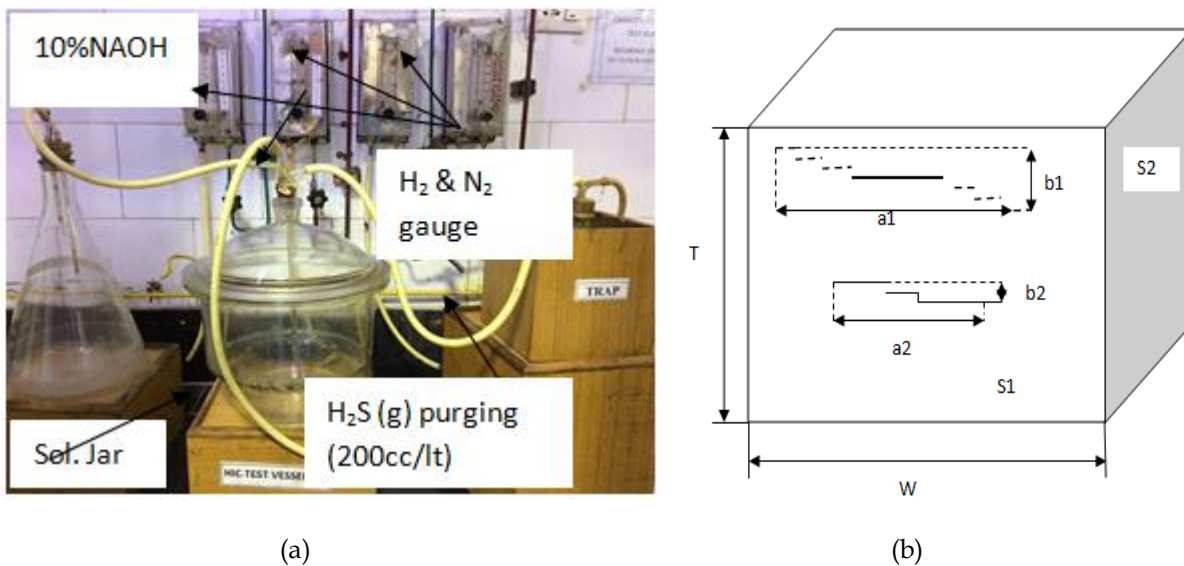

(a)   (b)

Figure 4.14: (a) HIC set-up; (b) Specimens dimensions to find crack lengths

4.7 CORROSION ANALYSIS OF HEAT TREATED X70 STEEL AND WELD SPECIMEN IN DIFFERENT EXPOSING ENVIRONMENT

Corrosion behaviour of heat treated X70 specimen in freshwater, seawater, and sodium thiosulphate solution (10^{-3} mol/l or 10^{-2} mol/l) studied by weight loss method. ASTM G1-03 standard was used to find the corrosion rate of heat treated specimen after exposure of thirty days interval.

4.7.1 Specimen preparation

API X70 steel was used to find corrosion behavior by weight loss and electrochemical tests. For weight loss corrosion testing the twenty four specimen of dimensions 12x10x22 mm were cut from parent metal of size 290x290x22mm and then polished with 80, 120, 220, 320, 420, 600 emery grit papers and after that exposed in different test environments such as freshwater (pH=7), seawater (pH=8.2) and sodium thiosulphate solution (10^{-3}mol/l, pH=5 & 10^{-2}mol/l, pH=3) for thirty days interval. Linear sweep voltammetry approach was used for

electrochemical corrosion testing of seven weld specimens of size 25x20x22 mm in seawater and sodium thiosulphate solution (10^{-3}mol/l & 10^{-2}mol/l).

4.7.2 Heat treatment method for weight loss study

For corrosion testing by the weight-loss method, the base metal specimen (API X70 steel) was heat treated. Two heat treatment procedures (HT-1 & HT-2) were used to study the corrosion behavior of API X70 steel in different test solutions such as freshwater (pH=7), seawater (pH=8.2), and sodium thiosulphate solution (10^{-3}mol/l, pH=5 & 10^{-2}mol/l, pH=3). For heat treatment, three main steps were used i.e., austenitizing, quenching, and then tempering. In this procedure, tempering temperature is varied (from 300° C, 450° C, and 600° C) to see its effect on the corrosion rate. In HT-1 and HT-2, the autenizing temperature taken 1000° C and 850° C. For enhancing the corrosion resistance of as received API X70 linepipe steel in sour applications, an appropriate heat treatment cycle was designed to get adequate mechanical and microstructural properties. Table 4.9 shows the suitable heat treatment method with the distribution of the number of samples immersed in four test solutions.

Table 4.9: Heat treatment method with sample-wise distribution in test environments

Heat treat ment	Austenizing Temp./time ($^{\circ}$C/min)	Tempering Temp./time ($^{\circ}$C/min)			Test Solution/Sample			
		300°	450°	600°	FW (pH=7)	SW (pH=8.2)	5%NaCl + 10^{-2} m/l STS (pH=3)	5%NaCl + 10^{-3} m/l STS (pH=5)
BM	----	-----	-----	-----	2 S	2 S	2 S	2 S
HT-1	1000°C/30min	1hr	1 hr	1 hr	2 S	2 S	2 S	2 S
HT-2	850°C/30min	1hr	1 hr	1 hr	2 S	2 S	2 S	2 S

Note: BM: Base metal; FW: Fresh water; SW: Sea water; 10^{-2}mol/l and 10^{-3}mol/l sodium thio-sulphate solution; S: no of specimen; STS: Sodium Thio-sulphate solution.

4.7.3 Linear sweep voltammetry technique for weld joint corrosion study

Linear sweep voltammetry technique of electrochemical corrosion was used to study the corrosion behavior of seven weld specimens. Electrochemical testing performed in a potentiostat-galvanostatic auto lab setup having three conventional electrode cells, such as an auxiliary electrode, reference electrode, and working electrode. Ag-AgCl$_2$ used as an auxiliary electrode; the platinum wire used as a reference electrode and work specimen used as a working electrode. The corrosion scan rate of 1mVs-1 was used to study the corrosion behavior of weld specimens in different test solutions. Corrosion behavior of weld specimen in different test solutions such as seawater (pH=8.2) and sodium thiosulphate solution (10^{-3}mol/l, pH=5 & 10^{-2}mol/l, pH=3) observed.